Inorganica Chimica Acta 558 (2023) 121718

Contents lists available at ScienceDirect

Inorganica Chimica Acta

journal homepage: www.elsevier.com/locate/ica

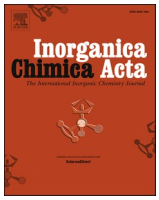

Self-metalation of tetraphenyl porphyrin on Au(111): Structural characterisation *via* X-ray standing wave analysis

Eleanor S. Frampton [a,b,1], Matthew Edmondson [a], Chris J. Judd [a], David A. Duncan [c], Robert G. Jones [b], Alex Saywell [a,*]

[a] School of Physics & Astronomy, University of Nottingham, Nottingham NG7 2RD, UK
[b] School of Chemistry, University of Nottingham, Nottingham NG7 2RD, UK
[c] Diamond Light Source, Harwell Science and Innovation Campus, Didcot OX11 0QX, UK

ARTICLE INFO

Keywords:
Tetraphenyl porphyrin
Au(111)
Scanning probe microscopy
Normal incidence x-ray standing wave (NIXSW)
X-ray photoelectron spectroscopy (XPS)
On-surface synthesis

ABSTRACT

The study of surface-confined reactions provides a route towards characterising the mechanistic processes which underpin heterogeneous catalysis. On-surface reactions provide alternative pathways to solution phase synthesis, and can be studied by a range of techniques which can provide chemical and structural information. Importantly, these kinds of studies give us the insight required to potentially control the selectivity and efficiency of these reactions, as well as allowing for the design of molecular systems with specific functionalities. Porphyrin molecules are frequently selected as participants in these systems as they offer significant customisability, with respect to the reactivity of pendant groups and metal atoms which can be incorporated within the porphyrin macrocycle. Utilising the normal incidence X-ray standing wave (NIXSW) technique in conjunction with scanning probe methods and X-ray photoelectron spectroscopy (XPS) enables the generation of detailed models of on-surface systems, including the adsorption geometries of individual molecules. Here the NIXSW technique has been used to perform structural characterisation of three distinct phases of an on-surface reaction of tetraphenyl porphyrin (TPP) on Au(111); close-packed, diffuse and metalated. Using the chemical specificity of XPS and NIXSW we gain insight into chemical and structural changes exhibited by nitrogen atoms within the porphyrin macrocycle at several stages within the reaction process.

1. Introduction

Porphyrin molecules are biologically active and commonly found in many natural systems, and are key components of both photosynthesis and oxygen carriers in red blood cells. They also have a rich synthetic chemistry, can be easily functionalised, and display high thermal stability [1]. Functionalised porphyrin molecules are known to undergo a range of on-surface reactions (including Ullmann- and Glaser-type coupling [2,3]). Even 'simple' porphyrins, such as tetraphenyl porphyrin (2H-TPP - see Fig. 1), can participate in multiple on-surface processes given the correct conditions, [4] including; self-metalation [5,6], ring-closing [7,8], and covalent coupling [9,10].

A highly-successful approach for studying such systems is to employ a combination of scanning probe microscopy (SPM) and X-ray photoelectron spectroscopy (XPS) to provide both real-space lateral resolution and chemical sensitivity [11,12]. This combination takes the best features of SPM and XPS, while ameliorating some of the inherent issues with each technique (e.g. a lack of comprehensive chemical identification from SPM, and the requirement for ensemble averaging within XPS). For example, while non-contact atomic force microscopy (nc-AFM) is an incredibly powerful technique for studying on-surface reactions with resolution down to the level of single chemical bonds [13], characterising the structure of non-planar molecules by scanning tunnelling microscopy (STM) or nc-AFM presents significant issues. In contrast, normal incidence X-ray standing wave (NIXSW) analysis combines the chemical specificity of XPS with the picometer-level spatial resolution provided by diffraction based techniques to allow detailed structural characterisation; with the exact adsorption sites of atomic species relative to the crystallographic planes of the substrate being obtained [14,15]. Various on-surface processes have been elucidated by NIXSW analysis; for example, details of Ullmann coupling [16], molecular conformations at the surface [17–19], the interaction

* Corresponding author.
E-mail address: Alex.Saywell@Nottingham.ac.uk (A. Saywell).
[1] Current Address: Max IV Laboratory, Fotongaten 2, 224 84 Lund, Sweden.

https://doi.org/10.1016/j.ica.2023.121718
Received 30 April 2023; Received in revised form 20 July 2023; Accepted 9 August 2023
Available online 11 August 2023
0020-1693/© 2023 The Author(s). Published by Elsevier B.V. This is an open access article under the CC BY license (http://creativecommons.org/licenses/by/4.0/).

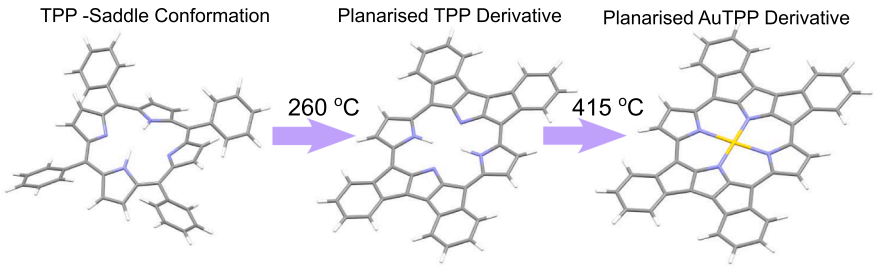

Fig. 1. On-surface reaction scheme of tetraphenyl porphyrin. Initial saddle conformation of 2H-TPP adsorbed on gold, followed by the planarised derivative which is produced upon heating to 250°C, followed by the final product, the planarised porphyrin derivative, metalated with a gold atom from the surface, which occurs at 415°C.

between the substrate and adsorbed species [20,21], and the ligation of gas molecules [22]. Therefore a combination of these approaches has significant benefits.

Porphyrin molecules have previously been shown to undergo a series of on-surface reactions, which can be effectively studied using XPS and NIXSW [23,18]. The chemistry of these systems may be studied using these methods due to the well defined N 1s core level signal in the XPS spectrum of the chemically active nitrogens within the porphyrins. Porphyrin molecules have two nitrogen environments within the core of the macrocycle; iminic (=N-) and aminic (-NH-). This produces two well-defined peaks within the nitrogen region of XP spectra, and as such, changes to the chemistry of the macrocycle will be reflected in these spectroscopic features. Metalation of porphyrin molecules has been observed *via* the uptake of a metal atom from the surface in addition to sequestration of separately deposited of metal atoms. Self metalation of porphyrins can be observed using STM, but it can be definitively characterised using XPS (the aminic and iminic features reduce to a single peak when all N atoms bond to a central metal atom [5,6,24]). Here, we build upon our previous work describing a combined XP spectroscopy and STM study characterising tetraphenyl porphyrin (labelled here as TPP) on Au(111) [25]. Three phases of TPP were reported and characterised using STM, scanning tunneling spectroscopy (STS) and XPS; a 'close packed' (as deposited) phase, a ring-closed species existing within a 'diffuse' phase, and a 'metalated phase' (consisting of Au-TPP) - see Fig. 1. Our characterisation of the close packed, diffuse and metalated phases of TPP on Au(111) are in excellent agreement with previous studies on similar porphyrin systems on coinage metals [7,26,27]. In the present study NIXSW is employed to determine the position of nitrogen species within TPP with respect to the Au(111) surface at distinct stages within an on-surface process; providing insight into the structure of the different surface-confined species in each phase, and the mechanisms through which they are formed.

2. Experimental methods

NIXSW and XPS measurements were performed on the I09 beamline [28] at the Diamond Light Source. Au(111) was prepared under ultra-high vacuum (UHV) conditions, at a base pressure of 4×10^{-10} mbar, via cycles of sputtering and annealing (sputter: 1 keV for 30 min, anneal: to 690 K for 30 min). The resultant clean gold surface was characterised with XPS and low-energy electron diffraction (LEED). TPP was deposited by exposing the clean Au(111) surface, held at room temperature, to the flux from a Knudsen-type evaporator held at 280 °C for 30 min. The close-packed phase of TPP forms following deposition onto the clean surface, with the diffuse and metalated phases produced upon heating to 260 °C and 415 °C, respectively. Each phase was characterised using LEED, XPS and NIXSW.

The I09 beamline utilises two undulator sources; one of which covers the soft X-ray range (100–2000 eV), which we refer to as XPS, and another which covers the hard X-ray range (2100–18000 eV), termed 'hard XPS' or HAXPES. The 'hard X-rays' were monochromated by a Si double crystal monochromator, and the 'soft' X-ray beam by a plane grating monochromator. The XP spectra were acquired using a VG Scienta EW4000 HAXPES analyser which is mounted perpendicular to the incoming light (light is linearly polarized in the horizontal plane). The binding energies were defined relative to the Fermi level of the substrate. The reflectivity curves were obtained from a fluorescent plate mounted in the port through which the synchrotron light is incident. The curves were then acquired using a CCD camera mounted on a window opposite the port. These reflectivity curves were fitted to determine the phase of the X-ray standing wave in addition to modelling peak broadening due to experimental uncertainties. Non-dipolar effects in the photoelectron yield were modelled using a backward-forward asymmetry parameter, Q, derived from the calculations of Nefedov et al. [29,30]. Due to the large acceptance angle of the EW4000 analyser (±30°) an effective emission angle of 15° was used for (111), with respect to the surface plane.

N 1s core level XP spectra were obtained using photon energies of 900 eV. NIXSW measurements were acquired from the (111) reflection plane (using nominal energies of $E_{Bragg} = 2631$ eV). Each NIXSW measurement was repeated at least three times, with each new measurement performed at a different sample location to avoid beam damage. Before and after each measurement, core level spectra for the N 1s and C 1s ($h\nu = 900$ eV) were obtained in order to monitor possible beam damage, with no significant changes observed (no observable chemical shift and less than noise level, $\sim 10\%$, change in peak intensities). A reflectivity curve was measured prior to each X-ray standing wave measurement, to check the quality of the new areas of the surface and ensure that the energy range of each spectrum is the same with respect to the Bragg energy. The XP spectra acquired during the XSW measurement are fit using a combination of Gaussian and Doniach-Šunjić line shapes [31], allowing chemically distinct species to be addressed at each photon energy.

3. Results and Discussion

NIXSW is a technique utilised to determine the structure of molecule–substrate systems, allowing the adsorption sites of the specific atoms within these molecules, and their 'heights' above the surface, to be calculated. The phases of TPP on Au(111) have been previously described using XPS, and the chemical states present in each phase have been identified [25]. This background allows us to employ chemically sensitive NIXSW to determine structural details of this system by focusing on the N 1s signatures from the aminic and iminic nitrogen atoms within TPP. NIXSW measurements are facilitated by matching the energy of photons incident upon a crystalline substrate with the Bragg condition for a given Bragg reflection, $H = (h,k,l)$. Under these conditions an X-ray standing wave is formed, and the location of maximum intensity can be varied along the direction $[h,k,l]$ by small changes in the photon energy. As the position of maximum intensity is moved, any atom immersed in the standing wave will be subjected to varying electromagnetic field intensity as a function the position of the standing wave maxima, and a characteristic adsorption profile may be obtained

(here we monitor the photoelectron intensity resulting from X-ray adsorption). The measured profile may be fitted, using dynamical diffraction theory, with two dimensionless parameters, coherent fraction (C_f) and coherent position (C_p) [14]. The coherent fraction is a measure of the distribution of adsorption distances from the crystal plane being used. For a given plane, this can be used to infer the distribution of adsorption sites in the system ($C_f \approx 1$ suggests a single adsorption site, with $C_f \approx 0$ suggests multiple sites or a random ordering). The coherent position can generally be considered as the mean adsorption height ($d_{h,k,l}$) expressed as a function of the separation of the (h,k,l) planes, $D_{h,k,l}$, such that: $d_{h,k,l} = (n + C_p).D_{h,k,l}$, where n is an integer [14,15].

From the N 1s region of the XPS we can identify the nitrogen environments present and use them to characterise the phases of TPP on Au (111). Here we identify three phases, and a total of five relevant nitrogen environments: The aminic and iminic in saddle-shaped TPP; the aminic and iminic in TPP adsorbed above an adatom (aaTPP); and the single nitrogen environment within metalated TPP. Fig. 2 outlines the sample preparation and characterisation for these three distinct phases.

Fig. 2a illustrates the sample preparation required to produce the close-packed, diffuse, and metalated phases of TPP on Au(111) (STM topographs of the close-packed and diffuse phases are shown in Fig. 2b and c, respectively). Fig. 2d-f shows N 1s XP spectra for each stage of the reaction and corresponding peak fitting. Along the lines of previous work [25] we assign peaks at binding energies (BE) of 397.2 eV and 399.4 eV to the iminic and aminic nitrogen environments for a saddle-shape porphyrin on Au(111) (see Table 1, labelled as N_α and NH_α). The $\sim$ 2 eV difference in BE is consistent with previously reported studies of porphyrin species [32]. The smaller peaks at 397.8 eV and 400.1 eV (labelled as N_β and NH_β) are assigned to TPP above an Au adatom; previously identified using a combination of STM and density functional theory (DFT) [33,34]. Following annealing the diffuse phase is formed, with peaks assigned to $N_\alpha, NH_\alpha, N_\beta$ and NH_β species. The relative abundance of the α and β species depends sensitively upon sample preparation, annealing conditions and location on the surface; in line with the expectation that the availability of Au adatoms is related to the surface temperature. The metalated phase is typified by a dominant peak at 398.0 eV BE (N_μ).

These distinct chemical environments allow us to perform chemically sensitive NIXSW measurements. Importantly, the relative composition of the α and β nitrogen species can be defined by the peak areas obtained within the XPS measurements (see Table 1).

3.1. Close-packed phase

Firstly, we detail the close-packed phase of TPP on Au(111) (Fig. 2b) as characterised by STM. We observe an ordered self-assembled structure (dimensions of unit cell calculated from the LEED pattern are 1.4 × 1.4 nm [25]). As discussed above XPS analysis of the N 1s region reveals four distinct peaks. Importantly, NIXSW requires hard X-rays (HAXPES), in order to match the Bragg condition for diffraction, which results in a reduction in cross section of the nitrogen peaks and a corresponding reduction in signal to noise ratio. This reduction in sensitivity precludes resolving the α and β nitrogen environments (i.e. TPP and aaTPP species), although aminic and iminic nitrogen are clearly distinguished. Consequently, NIXSW profiles are only obtained for aminic and iminic nitrogen species.

The NIXSW profiles obtained for these two environments and the C_f and C_p values produced from this fitting were 0.25 ± 0.08 and 1.25 ± 0.07 for the iminic nitrogen (=N-) and 0.21 ± 0.08 and 1.35 ± 0.07 for the aminic nitrogen (-NH-) (See Table 2 and Fig. 3a).[2] In order to interpret the experimental C_f and C_p values in terms of adsorption heights we require a model of the molecular species present (detailing their adsorption heights and fractional abundance). A detailed description of the model is presented within the SI; In summary, our model is based upon the estimation of nitrogen adsorption 'heights' (relative to the (111) plane) derived from van der Waals (vdW) radii of nitrogen and gold. Consideration is given to the vertical displacement of aminic nitrogen relative to the iminic species, due to the expected saddle-shape conformation, as well as the previously observed presence of Au adatoms residing under the TPP species [25,34]. These model heights are converted to corresponding coherent position (C_p) values. The coherent fractions (C_f) are derived from (i) the experimentally determined ratio of TPP to adatom TPP (aaTPP - species adsorbed above a Au adatom) obtained from XPS measurements, and (ii) the experimentally observed ratio of nitrogen adsorption sites (with respect to the high-symmetry atop, bridge, and threefold hollow sites) obtained from STM measurements (as detailed within the SI).[3]

Having previously defined the ratio of aaTPP:TPP ($\beta : \alpha$) species present using XPS (see Table 1), we employ details from LEED and STM images to provide further basis for a model. LEED and STM analysis show that the self-assembled TPP structure forms an incommensurate lattice with respect to the Au(111) surface [33,25]. Analysis of STM images allows the location of nitrogen atoms, with reference to the high-symmetry adsorption sites (bridge, atop, threefold hollow), to be obtained. Our analysis indicates that a range of nitrogen adsorption sites are present (in line with previous LEED results demonstrating an incommensurate molecular overlayer), and that when we consider adsorption sites in terms of their proximity to the nearest high-symmetry site there is a roughly equal distribution between bridge, atop, threefold hollow locations (see SI). We have considered modelling nitrogen adsorption as a quasi-continuous distribution of sites between the highest (atop) and lowest (threefold hollow) sites, and do not find a significant difference when compared to a model considering only high-symmetry sites (see discussion within SI).

Our proposed model therefore utilises information on the abundance of adatom TPP species, and the proportion of high symmetry adsorption sites, in combination with values of adsorption heights derived from the van der Waals (vdW) radii gold and nitrogen. The calculated 'heights' for the distinct nitrogen environments at each high-symmetry adsorption site, atop, bridge and three fold hollow, can be used to determine expected C_p values (details of the model can be found in the SI). The relative occupation of different sites, and the relative abundance of the adatom species, determined experimentally, informs the fraction of each species (C_f) within our model. The resultant coherent fractions and positions for each species can be visualised on an Argand diagram, displayed as component vectors with polar coordinates, representing the heights and relative abundance of each atom adsorbing into a specific site (Fig. 3b,c). Here the pink, green and blue arrows show the calculated C_f (radii) and C_p (angle) for the threefold hollow, bridge, and atop adsorption sites (iminic N shown in Fig. 3b, and aminic shown in Fig. 3c). The red, cyan, and orange arrows correspond to adatom TPP species (i.e. aaTPP) in the high symmetry sites. The vector summation of all of the components gives rise to the predicted C_f and C_p for the system (black arrow); these may be compared directly with the experimentally obtained values.

We now compare our model to the experimentally obtained values of C_f and C_p. Fig. 3b and c show the experimental values (and associated error) as a red region, with the calculated total C_f and C_p for our model illustrated by the black arrow. A direct comparison between the experimental and calculated C_p values shows excellent agreement (see

[2] $C_p = d_{hkl}/D_{hkl}$ ($0 \leqslant C_p \leqslant 1$) where hkl is the Bragg reflecting plane, d_{hkl} is the atomic distance from the hkl planes and D_{hkl} is the layer spacing.

[3] Inclusion of a periodic vertical corrugation in the surface Au atom height, induce by the herringbone reconstruction (±0.1Å)[35], is expected to have a negligible effect (1 % decrease in coherent fraction) upon the modelled values.

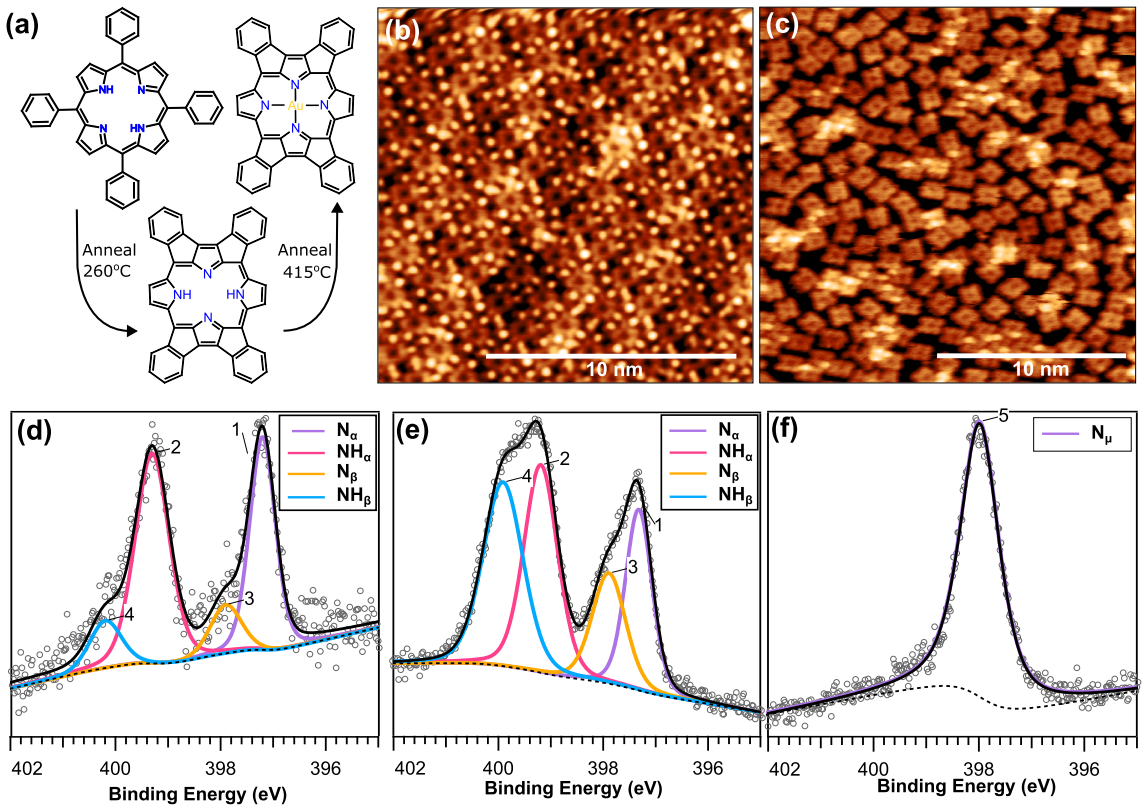

Fig. 2. Summary of previously observed on-surface reactions for TPP on Au(111); STM and XPS characterisation. (a) Reaction scheme showing structure of the porphyrin molecules at each stage of the reaction. The three phases are: close-packed phase (consiting of TPP in the saddle conformation), diffuse phase (consisting of planarised TPP), and metalated phase (metalised by incorporation of Au and loss of two hydrogen atoms from the porphryin core). STM topographs of (b) close-packed TPP arrangement [$V_{Sample} = 0.6$ V, $I_{Set-point} = 50$ pA], and (c) 'diffuse' phase of TPP on Au(111) formed following annealing [$V_{Sample} = 1.3$ V $I_{Set-point} = 5$ pA]. N 1s spectra of, (d) close-packed TPP, (e) the 'diffuse' phase of TPP, and (f) metalated TPP [Photon Energy $= 900$ eV].

Table 1
XPS N 1s core level peak positions for the three phases of TPP. Where N_α and NH_α are the iminic and aminic nitrogen atoms in saddle shaped TPP, N_β and NH_β are the aminic and iminic nitrogen atoms in TPP interacting with a gold adatom and N_μ is nitrogen bonding to gold in a metalated porphyrin.

	Binding Energy (eV)				
Data set	N_α	NH_α	N_β/N_μ	NH_β	$\alpha:\beta$ Ratio
Close-packed	397.2	399.4	397.8	400.1	9:4
Diffuse	397.3	399.1	397.7	400.1	2:1
Metalated			398.0		

Table 2
Table of coherent fraction and position parameters produced from both the experimental data and from the modelling using combinations of component vectors. C_p values are written as $\geqslant 1, < 2$ indicating that the nitrogen species reside in the second reflected plane.

Phase	**Peak**	Exp. C_f	Exp. C_p	Model C_f	Model C_p
Close-packed	-N=	0.25 ± 0.08	1.25 ± 0.07	0.34	1.25
	NH	0.21 ± 0.08	1.35 ± 0.07	0.34	1.34
Diffuse	-N=	0.41 ± 0.11	1.25 ± 0.07	0.29	1.26
	NH	0.37 ± 0.10	1.27 ± 0.07	0.34	1.27
Metalated	N-Au	0.46 ± 0.06	1.30 ± 0.04	0.48	1.28

Table 2); with a reduced agreement for C_f (likely due to an under estimate of the prevalence of the adatom TPP species). The difference in experimental values for the N and NH C_p is indicative of the saddle confirmation which TPP exhibits in bulk crystals and upon adsorption to metallic surfaces. The two sets of pyrrole rings are rotated in opposite directions, one set pointing up and the other down relative to the surface [36]. Here the aminic nitrogen atoms point upwards from the surface and the iminic point downwards, which is consistent with a model where the iminic nitrogen are able to interact with metallic substrates [18]. The coherent position values for the nitrogen peaks were 1.25 ± 0.07 for the iminic nitrogen (=N-) and 1.35 ± 0.07 for the aminic nitrogen (-NH-), with a difference of 0.1 (corresponding to a separation of 0.236 Å). This is in excellent agreement with the displacement between the aminic and iminic nitrogen atoms, 0.2 Å, obtained from previously reported crystallography data [37].

An adsorption model for the close-packed phase of TPP can be seen in Fig. 4. The iminic nitrogen atoms are located above the first empty (111) plane above the gold surface and are pictured here adsorbed in the atop position at a height of 3.21 Å (bridge, and threefold sites are also included within our model, see SI for values). The aminic nitrogen atoms are located within the second plane above the gold surface, pictured in a atop site at a height of 3.41 Å.

In summary, for the close-packed phase we find good agreement between the experimental data and our vdW-based adsorption model. The combination of the two TPP species being present, the saddle TPP and aaTPP is supported by this model. We identify the presence of saddle-shape conformation TPP molecules from the differences in coherent position between the aminic and iminic peaks.

3.2. Diffuse phase

Similar XSW analysis was performed for the diffuse phase of TPP on Au(111), in which two peaks were fit to the HAXPES data acquired within the XSW protocol; corresponding to the iminic nitrogen and aminic nitrogen environments (as for the close-packed phase the $\alpha:\beta$

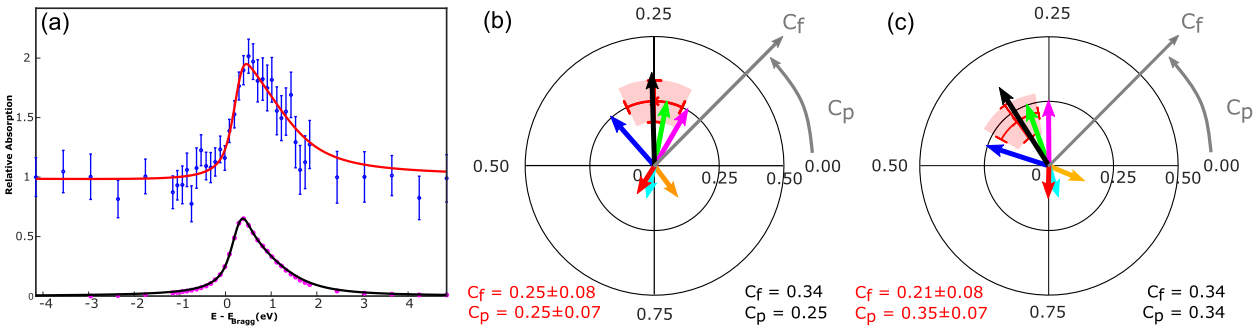

Fig. 3. (a) NIXSW measurements of the close-packed phase of TPP. NIXSW photoelectron yields obtained using the (111) reflection from the Au(111) crystal for the iminic N1 s signal. (b) and (c) Argand diagrams for iminic and aminic Nitrogen in close-packed phase showing C_f and C_p values obtained from XSW measurements from the (111) reflection for the close-packed phase of TPP. The coloured arrows represent vectors showing C_f and C_p values for the different binding sites and environments for the N atom, atop TPP (blue), atop aaTPP (orange) bridge TPP (green), bridge aaTPP (cyan) 3-fold hollow TPP (pink), three fold hollow aaTPP (red), the black arrow represents a vector which is a sum of the component vectors, and the red error bars and pink shaded error represent the experimentally obtained values.

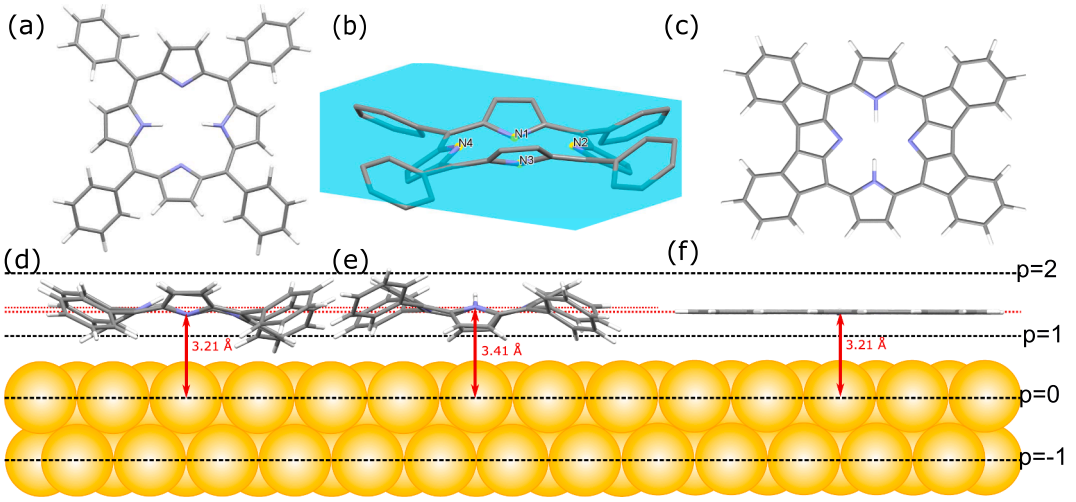

Fig. 4. Model of the close-packed phase of TPP on Au(111). (a) TPP in 'saddle' conformation; (b) taken from crystal structure reported in Ref [37]: blue plane defined using the four meso-carbon atoms, with N1 and N3 below the plane and N2 and N4 above. (c) Structure of a planar, ring-closed, derivative of TPP following cyclodehydrogenation. (d-f) Scheme showing two layers of surface gold atoms with the projected (111) crystal planes marked as dotted black lines; saddle-shaped conformation of TPP (within close-packed phase) on the surface highlighting the position of the iminic (d) and aminic (e) nitrogen is shown, with the structure of planar ring-closed TPP (within the diffuse phase) shown in (f).

ratio is used to determine the relative abundance of the aaTTP species). The corresponding XSW measurements produced structural parameters C_f and C_p (Table 2). A significant difference is observed, when comparing diffuse and close-packed phases, as the shift in coherent position for the aminic peak, bringing it in line with the coherent position of the iminic peak.

This supports our previously proposed mechanism, in which cyclodehydrogenation ring closing has occurred, causing the TPP molecules to form a planarised TPP derivative; the resulting reduction in interaction between TPP species (removal of Pi-Pi interactions) drives the transition to the diffuse phase [25]. This reaction has been reported for TPP on coinage metals, and observed *via* STM, resulting in a visible change in the structure of the porphyrin as well as an apparent 'flattening' of the molecule. The ring closing reaction can yield multiple products, depending on which carbon atom is dehydrogenated [7,38,39,8].

As for the close-packed phase we propose a model for the adsorption heights of the aminic and imminic nitrogen species (utilising the abundance of TPP and aaTPP species from XPS characterisation, and assuming an equal distribution of high-symmetry adsorption sites; a small contribution from AuTPP is also included within the model for the diffuse phase). The predicted values for C_f and C_p from our model are in agreement with the experimental values (see Table 2 and the Argand diagrams modelling this phase within the SI). The proposed structural model is shown in Fig. 4c and 4f. Our results indicates that both nitrogen species are now at a similar height in line with the previously proposed ring closing reaction.

3.3. Metalated phase

Following annealing to $415 \pm 50\ ^{\circ}C$ a metalated phase of TPP is observed; characterised by a single peak in the N 1s XP spectra (see Fig. 2), which is attributed to a metalated species in which all the nitrogen atoms coordinate to a central gold metal atom [5,40,41,27,6]. The NIXSW measurements of the (111) reflection for this phases yield coherent fractions and position parameters of $C_f = 0.46 \pm 0.06$ and $C_p = 1.30 \pm 0.04$ (see Fig. 5a). The absolute value of the coherent fraction in this phase is noticeably higher than in the close-packed or diffuse phases which is assigned to the reduced presence of aaTPP species.

As for the close-packed and diffuse phases, a disordered molecular assembly was assumed within our model (giving an equal distribution of high symmetry adsorption sites); here we do not include a contribution

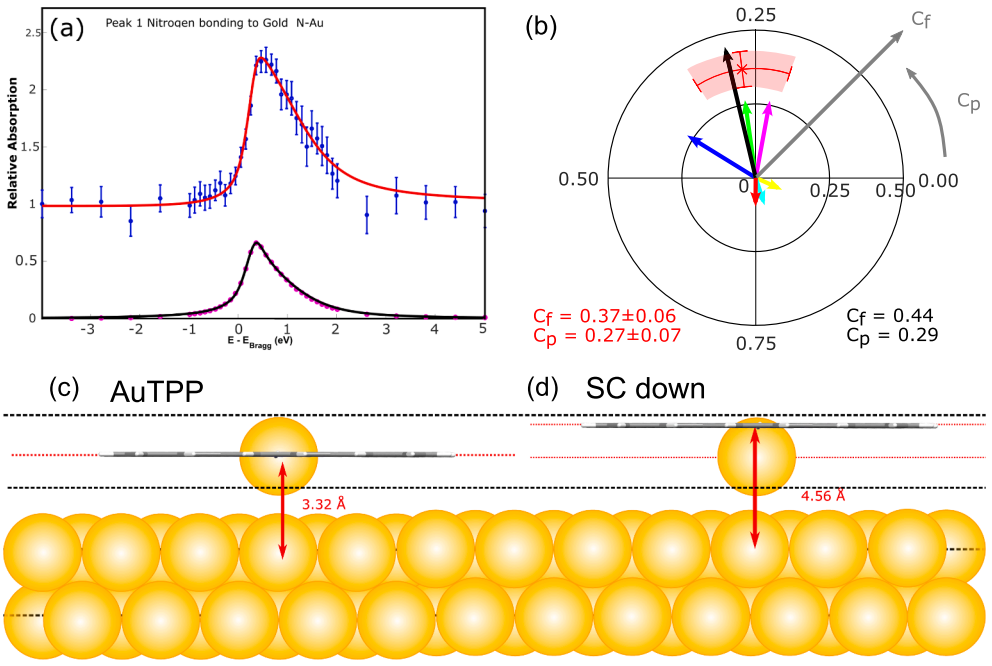

Fig. 5. XSW data and structural models of the metalated phase of TPP on Au(111). NIXSW measurements of the metalated phase of TPP. (a) NIXSW photoelectron yield obtained using the (111) reflection of the Au (111) crystal for the N1 s signal. (b) Argand diagram for the nitrogen species showing experimental C_f and C_p values (red region), component vectors for AuTPP (blue, green, pink) and SC Down species (red, cyan, yellow), and the sum of the component vectors (black arrow). (c) Model showing two layers of the gold surface with the (111) crystal planes marked in dotted black lines. A model of the metalated ring-closed derivative of TPP is shown in the second plane at a height of 3.32 Å above the surface. (d) Proposed model for the adsorption of the SC down metalated TPP sepecies.

from adatom adsorbed species as these species are not identified within XPS. A model where a single fully metalated TPP species (AuTPP) is formed leads to a predicted C_f considerably higher than the experimental value (see SI). An interpretation of this finding is that we have multiple adsorption heights, although one chemical environment. We rationalise this by considering an incomplete on-surface metalation reaction, where the Au atoms incorporated within the porphyrin macrocycle are not all co-planar with respect to the 'flat' porphyrin structure.

We develop a model based upon the published characterisation of SnPc on Cu(111), where the central Sn atom in the phthalocyanine molecule has been shown to sit either just above or just below the plane of the molecule to give a 'shuttlecock' shaped structure [42]. The Sn atom does not sit within the plane of the phthalocyanine molecule due to its large atomic radius (145 pm), and hence it sits either above or below. The atomic radius of the Au atom (174 pm) is larger than that of Sn, and of other metals commonly found within porphyrin molecules, meaning it may be possible for non-planar AuTPP to form [43]. However, crystallography data suggests that a planar Au-TPP complex is also stable [44]. We therefore propose that a mixture of planar AuTPP and 'shuttlecock' (SC) structures, where the atom is below the plane of the porphyrin species, may coexist on the surface. This represents an incomplete metalation of TPP following annealing, where AuTPP may be formed by the incorporation of metal atoms into the porphyrin core. A schematic of the proposed structures is presented in Fig. 5c,d. By varying the relative abundance of the SC and AuTPP species we find excellent agreement with our experimental data when 75% of the porphyrin species have been converted to AuTPP with 25% existing as a SC structure. [NB inclusion of a 'SC up' species does not improve the fit to experimental data, and the generation of such a structure is likely to be less facile than the 'SC down' variant].

4. Conclusion

The application of NIXSW characterisation to TPP on Au(111) provides structural details of three distinct phases of an on-surface reaction. The combination of XPS and NIXSW allows the chemical environments in each phase to be determined, and by probing these well-defined environments structural parameters (C_f and C_p) may be acquired by XSW analysis. These parameters were used to support structural models for each of the three phases; models were based upon physical properties of the atomic species (vdW radii), the relative abundance of molecular species (obtained via XPS), and estimates of adsorption site prevalence based upon previously published STM and LEED data. The models developed show good agreement with the reported data and provide details as to the reaction mechanism during the on-surface metalation of TPP.

Specifically, our analysis provides additional evidence for the 'saddle shape' geometry of TPP within the close-packed self-assembled phase on Au(111), and supports the presence of TPP adsorbed above gold adatom species. The convergence of the adsorption heights of the iminic (=N-) and aminic (-NH-) nitrogen species following anneal is in agreement with previously reported planarisation of TPP via a cyclodehydrogenation ring closing reaction. Further annealing gives rise to a single chemical environment for the nitrogen atoms within the porphyrin, indicative of a metalated AuTPP species, and we propose the coexistance of AuTPP in planar and 'shuttlecock' geometries, which results from incomplete metalation.

NIXSW analysis has afforded structural details of the TPP on Au(111) system which are not easily obtained *via* scanning probe methods. Using these methods in combination allows detailed structural information to be obtained for on-surface processes.

Declaration of Competing Interest

The authors declare that they have no known competing financial interests or personal relationships that could have appeared to influence the work reported in this paper.

Data availability

The experimental data on which this work is based can be found at https://dx.doi.org/10.17639/nott.7317

Acknowledgments

The authors would like to thank Diamond Light Source for time on Beamline IO9 under Proposal SI23730-1, and thank Pardeep K. Thakur for assistance. A.S. acknowledges support via a Royal Society University Research Fellowship.

Appendix A. Supplementary data

Supplementary data associated with this article can be found, in the online version, athttps://doi.org/10.1016/j.ica.2023.121718.

References

[1] R.A. Smith, The Colours of Life: An Introduction to the Chemistry of Porphyrins and Related Compounds (Milgrom, Lionel R.), J. Chem. Educ. 75 (4) (1998) 420.
[2] L. Grill, M. Dyer, L. Lafferentz, M. Persson, M.V. Peters, S. Hecht, Nano-architectures by covalent assembly of molecular building blocks, Nat. Nanotechnol. 2 (11) (2007) 687–691.
[3] C.J. Judd, D.V. Kondratuk, H.L. Anderson, A. Saywell, On-surface Synthesis within a Porphyrin Nanoring Template, Sci Rep 9 (1) (2019) 9352.
[4] J. Michael Gottfried, Surface chemistry of porphyrins and phthalocyanines Surf, Sci. Rep. 70 (3) (2015) 259–379.
[5] J. Michael Gottfried, K. Flechtner, A. Kretschmann, T. Lukasczyk, H.-P. Steinrück, Direct Synthesis of a Metalloporphyrin Complex on a Surface, J. Am. Chem. Soc. 128 (17) (2006) 5644–5645.
[6] T.E. Shubina, H. Marbach, K. Flechtner, A. Kretschmann, N. Jux, F. Buchner, H.-P. Steinrück, T. Clark, J. Michael Gottfried, Principle and Mechanism of Direct Porphyrin Metalation: Joint Experimental and Theoretical Investigation, J. Am. Chem. Soc. 129 (30) (2007) 9476–9483.
[7] B. Cirera, B. de la Torre, D. Moreno, M. Ondráček, R. Zboril, R. Miranda, Pavel Jelínek, David Écija, On-surface Synthesis of Gold Porphyrin Derivatives via a Cascade of Chemical Interactions: Planarization, Self-Metalation, and Intermolecular Coupling Chem. of Mater. 31 (9) (2019) 3248–3256.
[8] F. Bischoff, A. Riss, G.S. Michelitsch, J. Ducke, J.V. Barth, K. Reuter, Willi Auwärter, Surface-Mediated Ring-Opening and Porphyrin Deconstruction via Conformational Distortion, J. Am. Chem. Soc. 143 (37) (2021) 15131–15138.
[9] L. Lafferentz, V. Eberhardt, C. Dri, C. Africh, G. Comelli, F. Esch, S. Hecht, L. Grill, Controlling on-surface polymerization by hierarchical and substrate-directed growth Nature Chem 4 (3) (2012) 215–220.
[10] A. Saywell, A.S. Browning, P. Rahe, H.L. Anderson, Beton Beton, Organisation and ordering of 1D porphyrin polymers synthesised by on-surface Glaser coupling, Chem. Comm. 52 (68) (2016) 10342–10345.
[11] J.N. O'Shea, A. Saywell, G. Magnano, Lúıs M.A. Perdig̃ao, Christopher J. Satterley, Peter H. Beton, Vinod R. Dhanak, Adsorption of PTCDI on Au(111): Photoemission and scanning tunnelling microscopy, Surf. Sci. 603 (20) (2009) 3094–3098.
[12] J. Eichhorn, T. Strunskus, A. Rastgoo-Lahrood, D. Samanta, M. Schmittel, M. Lackinger, On-surface Ullmann polymerization via intermediate organometallic networks on Ag(111), Chem. Comm. 50 (57) (2014) 7680–7682.
[13] A. Sweetman, N.R. Champness, A. Saywell, On-surface chemical reactions characterised by ultra-high resolution scanning probe microscopy Chem, Soc. Rev. 49 (13) (2020) 4189–4202.
[14] D.P. Woodruff, Surface structure determination using x-ray standing waves Rep, Prog. Phys. 68 (4) (2005) 743–798.
[15] R.G. Jones, A.S.Y. Chan, M.G. Roper, M.P. Skegg, I.G. Shuttleworth, C.J. Fisher, G. J. Jackson, J.J. Lee, D.P. Woodruff, N.K. Singh, B.C.C. Cowie, X-ray standing waves at surfaces, J. Phys.: Condens. Matter 14 (16) (2002) 4059–4074.
[16] C.J. Judd, F.L.Q. Junqueira, S.L. Haddow, N.R. Champness, D.A. Duncan, R. G. Jones, A. Saywell, Structural characterisation of molecular conformation and the incorporation of adatoms in an on-surface Ullmann-type reaction, Commun Chem 3 (1) (2020) 166.
[17] P.J. Blowey, S. Velari, L.A. Rochford, D.A. Duncan, D.A. Warr, T.-L. Lee, A. De Vita, G. Costantini, D.P. Woodruff, Re-evaluating how charge transfer modifies the conformation of adsorbed molecules Nanoscale 10 (31) (2018) 14984–14992.
[18] P.T.P. Ryan, P.L. Lalaguna, F. Haag, M.M. Braim, P. Ding, D.J. Payne, J.V. Barth, T.-L. Lee, D.P. Woodruff, F. Allegretti, D.A. Duncan, Validation of the inverted adsorption structure for free-base tetraphenyl porphyrin on Cu(111), Chem. Comm. 56 (25) (2020) 3681–3684.
[19] P. Knecht, P.T.P. Ryan, D.A. Duncan, L.i. Jiang, J. Reichert, P.S. Deimel, F. Haag, J. T. Küchle, F. Allegretti, T.-L. Lee, M. Schwarz, M. Garnica, W. Auwärter, A. P. Seitsonen, J.V. Barth, A.C. Papageorgiou, Tunable Interface of Ruthenium Porphyrins and Silver, J. Phys. Chem. C 125 (5) (2021) 3215–3224.
[20] C.C. Silva, M. Iannuzzi, D.A. Duncan, P.T.P. Ryan, K.T. Clarke, J.T. Küchle, J. Cai, W. Jolie, C. Schlueter, T.-L. Lee, C. Busse, Valleys and Hills of Graphene on Ru (0001), J. Phys. Chem. C 122 (32) (2018) 18554–18561.
[21] A. Franco-Cañellas, Q. Wang, K. Broch, D.A. Duncan, P. Kumar Thakur, L. Liu, S. Kera, A. Gerlach, S. Duhm, F. Schreiber, Metal-organic interface functionalization via acceptor end groups, PTCDI on coinage metals Phys. Rev. Materials 1 (1) (2017). Article 013001.
[22] P. Knecht, J. Reichert, P.S. Deimel, P. Feulner, F. Haag, F. Allegretti, M. Garnica, M. Schwarz, W. Auwärter, P.T.P. Ryan, T.-L. Lee, D.A. Duncan, A.P. Seitsonen, J. V. Barth, A.C. Papageorgiou, Conformational Control of Chemical Reactivity for Surface-Confined Ru-Porphyrins Angew, Chem. Int. Ed. 60 (30) (2021) 16561–16567.
[23] C. Bürker, A. Franco-Cañellas, K. Broch, T.-L. Lee, A. Gerlach, F. Schreiber, Self-Metalation of 2H-Tetraphenylporphyrin on Cu(111) studied with XSW: Influence of the Central Metal Atom on the Adsorption Distance, J. Phys. Chem. C 118 (25) (2014) 13659–13666.
[24] K. Flechtner, A. Kretschmann, L.R. Bradshaw, M.-M. Walz, H.-P. Steinrück, J. M. Gottfried, Surface-Confined Two-Step Synthesis of the Complex (ammine) (meso-tetraphenylporphyrinato)-zinc(II) on Ag(111), J. Phys. Chem. C 111 (16) (2007) 5821–5824.
[25] M. Edmondson, E.S. Frampton, C.J. Judd, N.R. Champness, R.G. Jones, A. Saywell, Order, disorder, and metalation of tetraphenylporphyrin (2H-TPP) on Au(111) Chem, Commun. 58 (42) (2022) 6247–6250.
[26] G. Rojas, X. Chen, C. Bravo, J.-H. Kim, J.-S. Kim, J. Xiao, P.A. Dowben, Y.i. Gao, X. C. Zeng, W. Choe, A. Enders, Self-Assembly and Properties of Nonmetalated Tetraphenylporphyrin on Metal Substrates, J. Phys. Chem. C 114 (20) (2010) 9408–9415.
[27] M. Panighel, G.D. Santo, M. Caputo, C. Lal, B. Taleatu, A. Goldoni, Review of 2H-tetraphenylporphyrins metalation in ultra-high vacuum on metal surfaces, J. Phys.: Conf. Ser. 470 (2013), 012012.
[28] T.-L. Lee, D.A. Duncan, A Two-Color Beamline for Electron Spectroscopies at Diamond Light Source, Synchrotron Radiation News 31 (4) (2018) 16–22.
[29] C.J. Fisher, R. Ithin, R.G. Jones, G.J. Jackson, D.P. Woodruff, B.C.C. Cowie, Non-dipole photoemission effects in x-ray standing wavefield determination of surface structure, J. Phys.: Condens. Matter 10 (35) (1998) L623–L629.
[30] V.I. Nefedov, V.G. Yarzhemsky, I.S. Nefedova, M.B. Trzhaskovskaya, I.M. Band, The influence of non-dipolar transitions on the angular photoelectron distribution, J. Electron. Spectrosc. Relat. Phenom. 107 (2) (2000) 123–130.
[31] S. Doniach, M. Šunjić, Many-electron singularity in x-ray photoemission and x-ray line spectra from metals, J. Phys. C: Solid State Phys. 3 (2) (1970) 285–291.
[32] K. Diller, F. Klappenberger, M. Marschall, K. Hermann, A. Nefedov, Ch. Wöll, J. V. Barth, Self-metalation of 2H-tetraphenylporphyrin on Cu(111): An x-ray spectroscopy study, J. Chem. Phys. 136 (1) (2012). Article 014705.
[33] E. Frampton Self-assembly and on-surface chemistry of tetraphenyl porphyrin University of Nottingham (2021) PhD thesis.
[34] J. Mielke, F. Hanke, M.V. Peters, S. Hecht, M. Persson, L. Grill, Adatoms underneath single porphyrin molecules on Au(111), J. Am. Chem. Soc. 137 (5) (2015) 1844–1849.
[35] F. Hanke, Jonas Björk, Structure and local reactivity of the Au(111) surface reconstruction Phys, Rev. B 87 (23) (2013). Article 235422.
[36] S. Müllegger, M. Rashidi, T. Lengauer, E. Rauls, W.G. Schmidt, G. Knör, W. Schöfberger, R. Koch, Asymmetric saddling of single porphyrin molecules on Au (111), Phys. Rev. B 83 (16) (2011). Article 165416.
[37] P.M. Cantos, C.L. Cahill, A family of UO2(2+)–5-Nitro-1,3-dicarboxylate Hybrid Materials: Structural Variation As a Function of pH and Structure Directing Species, Cryst. Growth Des. 14 (6) (2014) 3044–3053.
[38] A. Wiengarten, J.A. Lloyd, K. Seufert, J. Reichert, W. Auwärter, R. Han, D. A. Duncan, F. Allegretti, S. Fischer, S.C. Oh, Ö. Sağlam, L.i. Jiang, S. Vijayaraghavan, D. Écija, A.C. Papageorgiou, J.V. Barth, Surface-Assisted Cyclodehydrogenation; Break the Symmetry, Enhance the Selectivity, Chem. Eur. J. 21 (35) (2015) 12285–12290.
[39] N. Cao, A. Riss, E. Corral-Rascon, A. Meindl, W. Auwärter, M.O. Senge, M. Ebrahimi, J.V. Barth, Surface-confined formation of conjugated porphyrin-based nanostructures on Ag(111), Nanoscale 13 (47) (2021) 19884–19889.
[40] M. Röckert, S. Ditze, M. Stark, J. Xiao, H.-P. Steinrück, H. Marbach, O. Lytken, Abrupt Coverage-Induced Enhancement of the Self-Metalation of Tetraphenylporphyrin with Cu(111), J. Phys. Chem. C 118 (3) (2014) 1661–1667.
[41] F. Buchner, V. Schwald, K. Comanici, H.-P. Steinrück, H. Marbach, Microscopic Evidence of the Metalation of a Free-Base Porphyrin Monolayer with Iron, ChemPhysChem 8 (2) (2007) 241–243.
[42] Y. Zhang, Y. Wang, J.-T. Lü, M. Brandbyge, R. Berndt, Mechanochemistry Induced Using Force Exerted by a Functionalized Microscope Tip, Angew. Chem., Int. Ed. 56 (39) (2017) 11769–11773.
[43] D. Qin, X.-J. Ge, Jing-Tao Lü, Tin-phthalocyanine adsorption and diffusion on Cu and Au (111) surfaces: A density functional theory study, Surf. Sci. 671 (2018) 6–10.
[44] A.M. Shachter, E.B. Fleischer, R.C. Haltiwanger, The Structure of (5,10,15,20-Tetraphenylporphinato)gold(III) Tetrachloroaurate(Ill), Acta Cryst. C 43 (10) (1987) 1876–1878.